Orientational ordering in the nematic phase of a polyethylene glycol–peptide conjugate in aqueous solution

Ian W. Hamley,* Marta J. Krysmann, Gemma E. Newby, and Valeria Castelletto
Department of Chemistry, University of Reading, Whiteknights, Reading RG6 6AD, United Kingdom

Laurence Noirez
CEA-CNRS Laboratoire Léon Brillouin, F91191 Gif-sur-Yvette, France
(Received 12 March 2008; published 18 June 2008)

The orientational ordering of the nematic phase of a polyethylene glycol (PEG)–peptide block copolymer in aqueous solution is probed by small-angle neutron scattering (SANS), with the sample subjected to steady shear in a Couette cell. The PEG-peptide conjugate forms fibrils that behave as semiflexible rodlike chains. The orientational order parameters $\bar{P}_2$ and $\bar{P}_4$ are obtained by modeling the data using a series expansion approach to the form factor of uniform cylinders. The method used is independent of assumptions on the form of the singlet orientational distribution function. Good agreement with the anisotropic two-dimensional SANS patterns is obtained. The results show shear alignment starting at very low shear rates, and the orientational order parameters reach a plateau at higher shear rates with a pseudologarithmic dependence on shear rate. The most probable distribution functions correspond to fibrils parallel to the flow direction under shear, but a sample at rest shows a bimodal distribution with some of the rodlike peptide fibrils oriented perpendicular to the flow direction.

DOI: 10.1103/PhysRevE.77.062901 PACS number(s): 87.14.em, 87.15.bk, 61.05.cf, 61.30.Gd

In a nematic phase, the molecules or particles have orientational but not translational order. Nematic phases are formed by molecules or particles with sufficient anisometry and have been observed for organic molecules, i.e., thermotropic liquid crystals as used in liquid crystal displays [1], wormlike micelle surfactant solutions [2–4], mineral nanoparticles [5,6], DNA [7,8], rodlike viruses [9], and peptides [10–12] among other systems. Nematic phases are fluid but have properties that are anisotropic (such as birefringence) on a macroscopic scale. Consequently the nematic phase is highly susceptible to alignment imposed by applied fields such as electromagnetic or mechanical fields. There are numerous studies on the orientation of nematic phases in magnetic and electric fields due to the use of thermotropic liquid crystals in displays, for example. There have been fewer structural studies on flow alignment of nematic phases. The alignment of the thermotropic liquid crystal 4-*n*-octyl-4′-cyanobiphenyl was investigated in Couette flow by small-angle x-ray scattering (SAXS) [13]. Later, Panizza *et al.* correlated the viscosity of the same mesogen in the smectic phase under Couette shear with changes in the orientation as probed by SAXS. The flow alignment was also studied in nematic and smectic phases under capillary flow by SAXS [14].

The present paper presents an analysis of the orientational ordering of a polyethylene glycol (PEG)–peptide conjugate in the nematic phase as studied by small-angle neutron scattering (SANS). The phase behavior of the conjugate is reminiscent of other rigid or semiflexible rodlike molecules such as DNA or poly(γ-benzyl-L-glutamate), in that as concentration is increased successively nematic and hexagonal columnar phases are formed [15,16]. This was confirmed by a combination of polarized optical microscopy with SANS and SAXS. In our PEG-peptide conjugate, the peptide is a modified fragment of the amyloid β (Aβ) peptide, specifically KLVFF (Aβ 16–20) extended by two phenylalanine residues at the nitrogen terminus to FFKLVFF. Here amino acids are denoted F phenylalanine, K lysine, L leucine, and V valine. This peptide is highly hydrophobic but self-assembles into fibrils at low concentration in organic solvents [17]. Conjugation to polyethylene glycol (M_n=3300, M_w/M_n=1.04) confers water solubility. Flow alignment of the nematic phase was observed upon application of low-shear-rate steady shear. Here, orientational order parameters are obtained by analysis of the anisotropic form factor scattering using an approach based on a cylinder form factor. In contrast to other approaches to analyze small-angle scattering from nematic phases [5,18–20], the method does not rely on any assumption about the orientational distribution function.

The PEGylated conjugate was synthesized by solid phase peptide synthesis as described elsewhere [16]. The crude peptide was purified by reverse-phase high-performance liquid chromatography and molecular weight was determined by matrix-assisted laser desorption/ionization-time of flight mass spectroscopy (MALDI-TOF). The structure was confirmed by ^{1}H NMR. Small-angle neutron scattering was performed on the two-dimensional detector PAXY of the Laboratoire Léon Brillouin. Samples were placed in a quartz Couette cell (0.1 mm gap) which was used to apply steady shear [21]. Shear rates are defined as $\dot{\gamma}=\Omega\bar{R}/(R_0-R_1)$, where Ω is the angular velocity, $\bar{R}$ is the average radius, and R_0=19.0 mm and R_1=19.1 mm are the inner and outer radii. Shear rates applied were 0.1–4.0 s^{-1}. Measurements were performed at room temperature. Data were obtained with neutrons incident along the shear gradient direction (radial configuration) and along the shear direction (tangential configuration). Data shown here are for the radial configuration since the intensity was higher and the SANS pattern was not

*Author to whom correspondence should be addressed. Also at Diamond Light Source, Didcot, Oxon OX11 0DE, U.K.

influenced by edge effects from the Couette cell wall. The neutron wavelength was 12 Å. The sample-detector distance was fixed at 2.5 m. The corresponding q ($q=4\pi \sin\theta/\lambda$) range extends from 0.08 to 0.8 $Å^{-1}$. The SANS data were corrected for the cell efficiency using an incoherent scatterer.

The scattering from fibrils in a nematic phase may be analyzed using the form factor for oriented cylindrically symmetric particles. A convenient method to obtain orientational order parameters is to write the anisotropy of the single-particle scattering as a series expansion in Legendre polynomials [22],

$$I_s(q,\theta_q) = \sum_L a_L(q) P_L(\cos\theta_q), \quad L \text{ even}. \tag{1}$$

Here $q=|\mathbf{q}|$ and $\theta_q=\cos^{-1}(\mathbf{q}\cdot\hat{\mathbf{n}})$, with $\hat{\mathbf{n}}$ the direction of preferred orientation (i.e., the horizontal shear flow direction here), give the magnitude and polar orientation of q. The $P_L(\cos\theta_q)$ are Legendre polynomials, which serve as an orthogonal basis set. The restriction to even L results from the centrosymmetry of the particle. Equation (1) can be written in such a way that the dependence of the expansion coefficients $a_L(q)$ on particle structure and orientational order is specified. This derivation has been given elsewhere for discrete scattering systems and this method has been used to analyze small-angle scattering from conventional low-molar-mass nematogens [23–25], for which atomic coordinates are available. In the present case, we use theory developed for continuous cylindrically symmetric particles [22], in particular uniform circular cylinders. The form factor of unaligned peptide fibrils can be described very accurately using such a form factor, as shown in our previous work [16].

The expansion coefficients can be written as

$$a_L(q) = \bar{P}_L S_L(q), \tag{2}$$

where $\bar{P}_L$ denotes an Lth-rank orientational order parameter defined as the ensemble average of Legendre polynomials:

$$\bar{P}_L = \int P_L(\cos\beta) f(\beta) \sin\beta \, d\beta, \tag{3}$$

Here $f(\beta)$ denotes the singlet orientational distribution function and β is the angle between the particle symmetry axis and the direction of preferred orientation.

The terms $S_L(q)$ depend on particle structure. They are given by

$$S_L(q) = (2L+1)(-1)^{L/2} \int j_L(qr) P_L(\cos\theta) P(\mathbf{r}) d\mathbf{r}, \tag{4}$$

with the integral over the particle volume. The $j_L(qr)$ are spherical Bessel functions and r,θ specify the magnitude and orientation of an intraparticle vector in a particle-fixed frame. The term $P(\mathbf{r})$ denotes the Patterson function, which is the electron density autocorrelation function in the case of x-ray scattering.

For a circular cylinder of radius R and length Λ, the integral in Eq. (4) can be evaluated in cylindrical coordinates (l,z) as

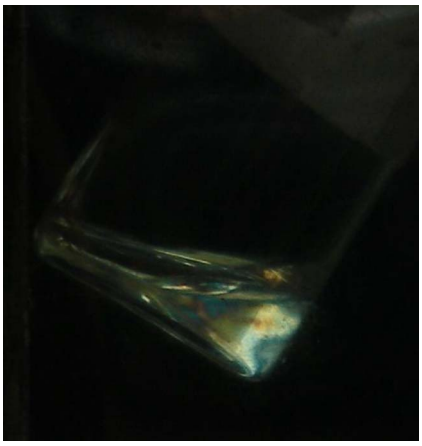

FIG. 1. (Color online) Fluid and birefringent nature of FFKLVFF-PEG, 5 wt % solution in D_2O. The sample in a vial is viewed between crossed polars.

$$S_L(q) = (2L+1)(-1)^{L/2} \int_{z=0}^{\Lambda} \int_{l=0}^{2R} P(l,z) j_L(q\sqrt{l^2+z^2}) \times P_L(z/\sqrt{l^2+z^2}) l \, dl \, dz. \tag{5}$$

Here, the Patterson function is given by [22]

$$P(\mathbf{r}) = P(l,z) = [2R^2 \cos^{-1}(l/2R) - l\sqrt{R^2-(l/2)^2}](\Lambda - z) \tag{6}$$

The model defined by Eq. (1) with the coefficients defined in Eqs. (2)–(6) was fitted to the experimental scattering data. Adjustable parameters were the orientational order parameters plus a scaling factor and a constant background term to allow for incoherent scattering background. The analysis was performed using a FORTRAN program; numerical integration was performed using a numerical algorithms group (NAG) library routine. Linear least-squares fitting was performed by solution of the normal equations using a matrix inversion routine (NAG libraries). Typically around 14 700 data points from a two-dimensional SANS pattern were included in the fit to each data set.

Polarized optical microscopy confirms the fluid and birefringent nature of the 5 wt % solution of FFKLVFF-PEG in D_2O studied (Fig. 1). In our analysis of the anisotropic SANS data from FFKLVFF-PEG, we have fixed the dimensions of the cylinders in the form factor model, using a radius 50 Å as determined previously [16] by fitting SAXS data in a dilute isotropic solution to the form factor of a uniform cylinder with low polydispersity, and also obtained from cryo transmission electron microscopy (TEM) images of the fibrils. The form factor model was that for infinite cylinders, since cryo-TEM indicates that the cylinders have a very long persistence length, at least several micrometers. Here, in order to evaluate Eqs. (2)–(6) we have taken $\Lambda = 500$ Å, consistent with a large Λ/R ratio. This persistence length may be an effective value, since TEM suggests a larger value [16]. However, increasing Λ led to a poorer fit, as quantified by χ^2 tests, while decreasing Λ led to unphysical values of $\bar{P}_4$ and a calculated scattering pattern shape

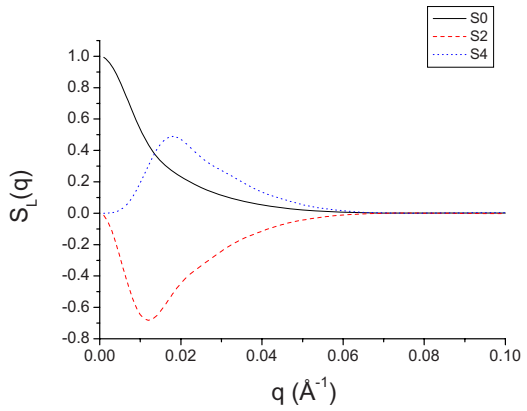

FIG. 2. (Color online) Coefficients of the form factor calculated for cylinders with $R=50$ Å, $\Lambda=500$ Å.

(elongated along the shear direction) that did not correspond to the one observed. Values of $\bar{P}_2$ decrease somewhat on increasing Λ, whereas $\bar{P}_4$ values decrease much more.

Figure 2 shows values of the expansion coefficients $S_L(q)$ that are determined by the dimensions of the cylinder. Reliable calculations could be performed in the experimental q range only for $L=0$, 2, 4. The integral in Eq. (5) did not converge reliably for higher L. We suspect this is because higher-order coefficients are extremely small. Further analysis is therefore restricted to these values of L.

Figure 3 shows measured and calculated small-angle neutron scattering patterns for the sample as loaded in the Couette cell prior to shearing and at relatively low and high shear rates. The development of anisotropy on increasing the shear rate is pronounced. The model describes the data very well and without systematic deviations (as quantified by plotting the residuals; not shown).

Figure 4 shows the orientational order parameters $\bar{P}_2$ and $\bar{P}_4$ obtained from the fits to the SANS data. As expected for a singlet orientational distribution function that decreases monotonically with β (up to $\beta=90°$), $\bar{P}_4<\bar{P}_2$. At rest, there is a small degree of initial orientation in the sample that is caused by loading into the Couette cell. On application of steady shear, there is a rapid increase in the magnitude of both order parameters up to $\dot{\gamma}=0.5$ s^{-1}, followed by regime with a much weaker shear-rate dependence (pseudologarithmic, see below). Higher shear rates were not accessible because the sample was expelled from the Couette cell. Following cessation of shear at $\dot{\gamma}=1$ s^{-1}, the order parameters $\bar{P}_2=(0.163\pm0.006)$ and $\bar{P}_4=(0.140\pm0.007)$ were determined. The $\bar{P}_2$ value is only slightly smaller than that obtained during shear; however, the $\bar{P}_4$ value is significantly increased. The effect on the orientational distribution function was probed by using the form of the distribution function that maximizes the entropy based on a given pair of values of $\bar{P}_2$ and $\bar{P}_4$ [25]:

$$f(\beta) = Z^{-1} \exp[a_2 P_2(\cos\beta) + a_4 P_4(\cos\beta)]. \quad (7)$$

Here Z is the normalization constant.

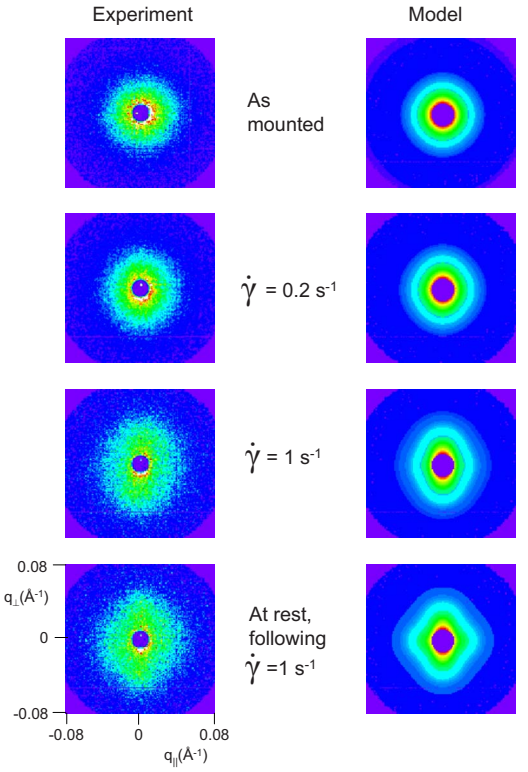

FIG. 3. (Color online) SANS data and model (on same intensity scale for each pair) under conditions as indicated. A small additional region of data at low q just outside the beamstop area was excluded in the models due to a contribution from stray scattering. The shear direction was horizontal.

Figure 5 compares the orientational distribution function during and after shear at $\dot{\gamma}=1$ s^{-1}. Under shear, a monotonically decaying $f(\beta)$ was observed; however, after shear there is a subsidiary maximum in $f(\beta)$ at $\beta=90°$. This indicates that a fraction of the PEG-peptide fibrils relaxed into an orientation perpendicular to the flow direction. There is in fact a subtle change in the shape of the SANS pattern during and

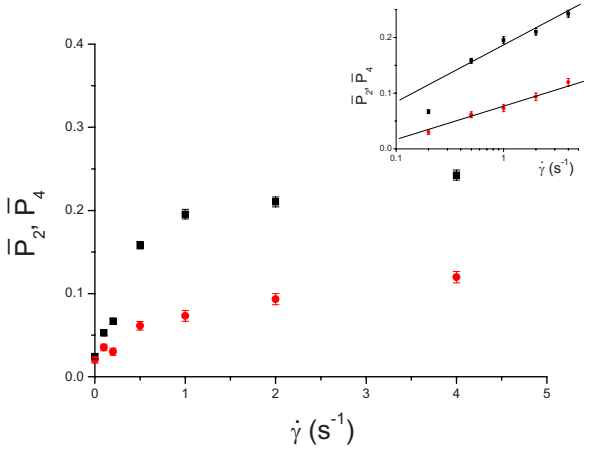

FIG. 4. (Color online) Shear-rate dependence of orientational order parameters $\bar{P}_2$ (■) and $\bar{P}_4$ (●). Inset: order parameters for higher shear rates plotted against logarithmic shear rate scale. The lines are guides to the eye.

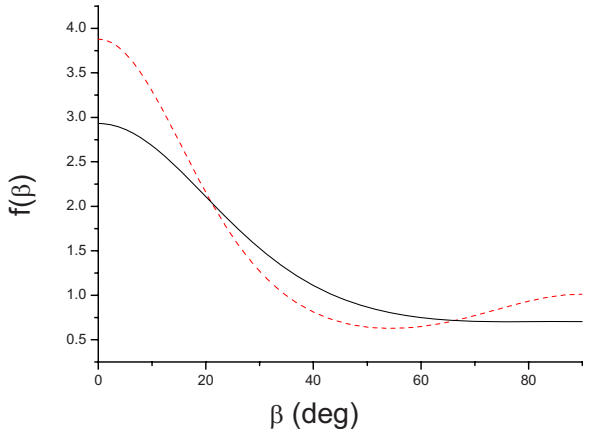

FIG. 5. (Color online) Orientational distribution function under shear at $\dot{\gamma}=1\ s^{-1}$ (solid black line) and following shear (dashed red line).

after shear (Fig. 3). After cessation of shear, the pattern developed a slightly "diamondlike" shape. However, a quantitative analysis requires detailed modeling as in the method we have outlined, which, being free of assumptions about the form of the orientational distribution function, can account for shape changes such as bimodal orientation states. We are not aware of prior studies on the shear-rate dependence of multiple-rank orientational order parameters in a nematic phase. There are detailed theories for shear-induced orientational order in nematic phases [26–28], and also for shear-induced phase separation of rodlike viruses or wormlike micelles [29–31]. In the former case, the dynamics of shear-induced alignment can lead to director instabilities including wagging and tumbling in appropriate shear regimes. We did not find evidence for any complex dynamics; however, it has to be considered that the time resolution of the SANS experiments is rather poor (each data set was acquired for 60 min). It would be interesting in future work to perform time-resolved experiments of the flow birefringence and rheology or orientational order via synchrotron SAXS. It would also be interesting to probe the concentration dependence of the orientational order parameters [20]. The shear-rate dependence of $\bar{P}_2$ at the isotropic-nematic phase transition has been measured for *fd* virus; the values of $\bar{P}_2$ are much larger than those reported here due to the higher shear rates studied (and higher rigidity of the virus particles), and there is a logarithmic dependence on shear rate [31]. As shown in Fig. 4 (inset) our data are consistent with this behavior, at least above a critical shear rate.

In summary, SANS reveals the shear-rate-dependent orientational ordering of a PEG-peptide conjugate that forms rodlike fibrils. The orientational order parameters were obtained from an anisotropic form factor model free of assumptions on the form of the orientational distribution function. Relaxation of orientation leads to a bimodal orientation distribution, whereas under shear a monotonically decaying $f(\beta)$ is observed.

[1] I. W. Hamley, *Introduction to Soft Matter*, revised ed. (Wiley, Chichester, U.K., 2007).
[2] C. Grand *et al.*, J. Phys. II **7**, 1071 (1997).
[3] I. A. Kadoma and J. W. van Egmond, Phys. Rev. Lett. **80**, 5679 (1998).
[4] E. Fischer and P. T. Callaghan, Phys. Rev. E **64**, 011501 (2001).
[5] B. J. Lemaire *et al.*, Europhys. Lett. **59**, 55 (2002).
[6] J.-C. P. Gabriel and P. Davidson, Top. Curr. Chem. **226**, 119 (2003).
[7] T. E. Strzelecka, *et al.*, Nature (London) **331**, 457 (1988).
[8] F. Livolant and A. Leforestier, Prog. Polym. Sci. **21**, 1115 (1996).
[9] S. Fraden, G. Maret, D. L. D. Caspar, and R. B. Meyer, Phys. Rev. Lett. **63**, 2068 (1989).
[10] V. Luzzati *et al.*, J. Mol. Biol. **3**, 566 (1961).
[11] A. Aggeli, I. A. Nyrkova, M. Bell, R. Harding, L. Carrick, T. C. B. McLeish, A. N. Semenov, and N. Boden, Proc. Natl. Acad. Sci. U.S.A. **98**, 11857 (2001).
[12] A. M. Corrigan, C. Müller, and M. R. H. Krebs, J. Am. Chem. Soc. **128**, 14740 (2006).
[13] C. R. Safinya, E. B. Sirota, and R. J. Plano, Phys. Rev. Lett. **66**, 1986 (1991).
[14] I. W. Hamley, V. Castelletto, and P. Parras, Phys. Rev. E **74**, 020701(R) (2006).
[15] M. J. Krysmann, I. W. Hamley, V. Castelletto, and L. Noirez, Adv. Mater. (Weinheim, Ger.) (to be published).
[16] I. W. Hamley *et al.*, Chem.-Eur. J. (to be published).
[17] M. J. Krysmann, V. Castelletto, and I. W. Hamley, Soft Matter **3**, 1401 (2007).
[18] A. J. Leadbetter and E. K. Norris, Mol. Phys. **38**, 669 (1979).
[19] R. Oldenbourg, X. Wen, R. B. Meyer, and D. L. D. Caspar, Phys. Rev. Lett. **61**, 1851 (1988).
[20] K. R. Purdy, Z. Dogic, S. Fraden, A. Rühm, L. Lurio, and S. G. J. Mochrie, Phys. Rev. E **67**, 031708 (2003).
[21] P. Baroni, C. Pujolle, and L. Noirez, Rev. Sci. Instrum. **72**, 2686 (2001).
[22] I. W. Hamley, J. Chem. Phys. **95**, 9376 (1991).
[23] R. W. Date *et al.*, Mol. Phys. **76**, 951 (1992).
[24] M. Kohli, K. Otnes, R. Pynn, and T. Riste, Z. Phys. B **24**, 147 (1976).
[25] I. W. Hamley *et al.*, J. Chem. Phys. **116**, 3887 (2002).
[26] T. Tsuji and A. D. Rey, Phys. Rev. E **57**, 5609 (1998).
[27] G. Rienäcker and S. Hess, Physica A **267**, 294 (1999).
[28] G. Rienäcker *et al.*, Physica A **315**, 537 (2002).
[29] P. D. Olmsted and C.-Y. D. Lu, Phys. Rev. E **60**, 4397 (1999).
[30] T. A. J. Lenstra, Z. Dogic, and J. K. G. Dhont, J. Chem. Phys. **114**, 10151 (2001).
[31] M. P. Lettinga and J. K. G. Dhont, J. Phys.: Condens. Matter **16**, S3929 (2004).